6328 *Chem. Mater.* **2010,** *22,* 6328–6340
DOI:10.1021/cm102140t

CHEMISTRY OF MATERIALS
Article

Nickel Sulfide Thin Films from Thio- and Dithiobiuret Precursors

Karthik Ramasamy, Mohammad A. Malik, Paul O'Brien,* James Raftery, and Madeleine Helliwell

The School of Chemistry and Manchester Materials Science Center, The University of Manchester, Oxford Road, Manchester M13 9PL, U.K.

Received July 30, 2010. Revised Manuscript Received September 18, 2010

The nickel(II) complexes of several 1,1,5,5-tetraalkyl-2-thiobiurets (R = methyl (**1**); methyl, ethyl (**2**); ethyl (**3**); isopropyl (**4**)) and 1,1,5,5-tetraalkyl-2,4-dithiobiurets (R = methyl (**5**); methyl, ethyl (**6**); ethyl (**7**)) have been synthesized. The single crystal X-ray structures of complexes (**1**), (**3**), (**4**), (**6**), and (**7**) have been determined. Thermogravimetric analysis shows all seven complexes decompose in a single step to one or another form of nickel sulfide. The complexes were used as single-source precursors for the deposition of nickel sulfide thin films by aerosol assisted chemical vapor deposition (AACVD) at temperatures between 320 and 480 °C. Complex (**1**) gave orthorhombic Ni_7S_6 at all temperatures with spherical tipped wirelike crystallites and plates. Complex (**2**) gave mixtures of hexagonal $Ni_{17}S_{18}$ and orthorhombic Ni_7S_6 with wires and plates. Complex (**3**) also led to a mixture of hexagonal $Ni_{17}S_{18}$ and orthorhombic Ni_7S_6 phases but with platelike crystallites. In contrast complex (**4**) gave orthorhombic Ni_9S_8 with flowerlike structures at 320 and 360 °C and branched structures at 400 °C. Complex (**6**) gave hexagonal $NiS_{1.03}$ at 360 and 400 °C, and orthorhombic Ni_7S_6 at 440 and 480 °C with wires and rods composed of spherical particles. Complex (**7**) gave rods composed of hexagonal plates with hexagonal $NiS_{1.03}$ phase at 360 and 400 °C and orthorhombic Ni_7S_6 at 440 and 480 °C. The composition of films deposited from all these complexes was confirmed by EDX analysis. The influence of the precursors on the nature of the deposited films is discussed.

Introduction

The phase diagram for the Ni−S system is more complex than that of the Fe or Co sulfides. In this system many crystalline phases and stoichiometries have been reported including the following: $Ni_{3+x}S_2$, Ni_3S_2, Ni_4S_{3+x}, Ni_6S_5, Ni_7S_6, Ni_9S_8, NiS, Ni_3S_4, and NiS_2.[1−3] Some compounds e.g. NiS and NiS_2 have been studied extensively, while for others only limited information is available.

NiS_2 (Vaesite) is a *p*-type semiconductor with a band gap of 0.5 eV. It is potentially useful in photo electrochemical solar cells,[4,5] IR detectors,[6] catalysts,[7] and sensors.[8] It is also used as a hydrodesulfurization catalyst and as a cathode material in rechargeable lithium batteries.[9] Nickel sulfide is considered as an "Achilles heel" in toughened glass, since it is responsible for glass cancer or spontaneous glass fracture. Rhombohedral Ni_3S_2 (heazlewoodite) is yellow in color and exhibits metallic properties. It has a slightly distorted body-centered cubic arrangement of sulfur with the metal atoms in some of the pseudotetrahedral holes.[10] At temperature above 556 °C, it converts to $Ni_{3+x}S_2$, with an fcc structure.[11] In this phase a substoichiometric number of metal atoms are randomly distributed in a cubic close packed structure of sulfur atoms with vacancies. The spinel structured Ni_3S_4 (polydymite), at higher temperatures > 400 °C, decomposes into NiS and NiS_2. At about 350 °C and 400 bar, Ni_3S_4 is converted into a hexagonal "NiAs- type" structure.[12,13]

Ni_7S_6 has been reported to exist in two polymorphic forms,[1] at higher temperature orthorhombic and at lower ones hexagonal, the phase transformation between these two polymorphs being sluggish. The crystal structure probably changes from hexagonal through monoclinic to orthorhombic as the stoichiometry changes, from Ni_9S_8 (through Ni_7S_6) to Ni_6S_5.[14]

Millerite NiS is useful as an IR detector and an electrode in PEC storage devices.[15] It has two polymorphs with unique properties.[16] At temperatures below 347 °C,

*Corrresponding author e-mail: paul.obrien@manchester.ac.uk.

(1) Kullerud, G.; Yund, R. A. *J. Petrol.* **1962**, *3*, 126.
(2) Swain, M. V. *J. Mater. Sci.* **1981**, *16*, 151.
(3) Barry, J. C.; Ford, S. *J. Mater. Sci.* **2001**, *36*, 3721.
(4) Sharon, M.; Tamizhmani, G.; Levy-Clement, C.; Rioux, J. *Sol. Cells* **1989**, *26*, 303.
(5) (a) Zainal, Z.; Saravanan, N.; Mien, H. L. *J. Mater. Sci: Mater. Electron* **2005**, *16*, 111. (b) Anuar, K.; Zainal, Z.; Saravanan, N.; Kartini, A. R. *AJSTD* **2004**, *21*, 19. (c) Anuar, K.; Zainal, Z.; Saravanan, N.; Zuriyatina, A.; Sharin, R. *Mater. Sci.* **2004**, *10*, 157. (d) Anuar, K.; Zainal, Z.; Saravanan, N.; Hamizi, S. N. *J. Indian Chem. Soc.* **2005**, *82*, 526.
(6) Leitz, S.; Hodes, G.; Tenne, R.; Manassen, J. *Nature* **1987**, *326*, 863.
(7) Oyama, S. T. *J. Catal.* **2003**, *216*, 343.
(8) Mane., R. S.; Lokhande, C. D. *Mater. Chem. Phys.* **2000**, *65*, 1.
(9) Cheon, J.; Talaga, D.; Zink, J. I. *Chem. Mater.* **1997**, *9*, 1208.
(10) Wold, A. *Adv. Chem. Ser.* **1971**, *98*, 17.
(11) Line, G.; Huber, M. *C. R. Acad. Sci.* **1963**, *256*, 3118.
(12) Lunovist, D. *Arkiy. Mineral. Geol.* **1947**, *A21*, 21.
(13) Kullerud, G. *Carnegie Inst. Washington Year Book* **1967**, *67*, 179.
(14) Gronvold, F.; Molleurd, R.; Rost, E. *Acta. Chem. Scand.* **1966**, *20*, 1997.
(15) Pramanik, P.; Biswas, S. *J. Solid State Chem.* **1986**, *65*, 145.
(16) Sparks, T.; Komoto, T. *Phys. Lett.* **1967**, *A25*, 398.

Published on Web 11/04/2010

NiS has rhombohedral symmetry (millerite), whereas at higher temperature it has the "NiAs-type" structure. In the rhombohedral form the nickel atom is surrounded by five sulfur atoms in tetragonal pyramidal coordination, while in the NiAs type, each nickel is octahedrally coordinated. Rhombohedral NiS is a semimetallic with temperature independent paramagnetism, whereas hexagonal NiS undergoes a first-order phase transition from a semiconducting antiferromagnetic phase to a metallic phase.[17]

Pramanik et al. have prepared nickel sulfide (NiS) films by solution growth on glass[15] or polymer substrates[18] and Anuar et al. electrodeposited (NiS).[5] In addition NiS films have been grown by successive ionic layer adsorption and reaction (SILAR),[19] laser ablation,[20] hydrothermal (Ni_3S_2, NiS),[21] soft solution-processing (NiS, Ni_3S_2, NiS_2, Ni_3S_4),[22] and CVD methods (NiS, NiS_2, Ni_7S_6).[23−27] Cheon et al. have reported the laser-driven photochemical vapor deposition of NiS from nickel bis(isopropylxanthate).[9] Nomura et al. studied the growth of $NiS_{1.03}$ from $[Ni(S_2CNEt_2)_2]$ on silicon (111) substrates by low-pressure chemical vapor deposition (LPCVD).[23] Alam et al. have used pyridine adducts of nickel(II) xanthates as single source precursors for the deposition of NiS thin films by AACVD.[24] Earlier, we have reported the deposition of nickel sulfide (NiS, NiS_2, Ni_7S_6) films from dithiocarbamate compounds of the type $[Ni(S_2CNRR')_2]$ where R,R′ = Et_2, MeEt, Me^{n}Bu, or Me^{n}Hex, by AA[25] and LPCVD methods[26] and also from xanthate compounds of the type $[Ni(S_2COR)_2]$ where R = Et or ^{i}Pr deposited NiS films by AACVD.[27] Recently Ni_9S_8 thin films and NiS, Ni_7S_6, and Ni_3S_2 nanoparticles have been deposited from bis(4-thiopent-3-ene-2-thionato)nickel(II) $[Ni(SacSac)_2]$.[28]

There are no reports on the deposition of nickel sulfide thin films from nickel complexes of thiobiuret or dithiobiuret except for our preliminary report.[29] Here we report the synthesis of the nickel(II) complexes of 1,1,5,5-tetraalkyl-2-thiobiuret (alkyl = methyl (**1**); methyl, ethyl (**2**); ethyl (**3**); isopropyl (**4**)) and 1,1,5,5-tetraalkyl-2,4-dithiobiuret (alkyl = methyl (**5**); methyl, ethyl (**6**); ethyl (**7**)) and the single crystal X-ray structure of complexes (**1**), (**3**), (**4**), (**6**), and (**7**). These compounds were used as single source precursors for the deposition of nickel sulfide thin films at relatively low temperature by AACVD. We also discuss the behavior of these two types of precursors toward the phase and the morphology of the deposited films.

Experimental Section

All preparations were performed under an inert atmosphere of dry nitrogen using standard Schlenk techniques. AR reagents were purchased from Sigma-Aldrich chemical company and used as received. Solvents were distilled prior to use. Mass spectra were recorded on a Kratos concept 1S instrument. Infrared spectra were recorded on a Specac single reflectance ATR instrument (4000−400 cm^{-1}, resolution 4 cm^{-1}). Elemental analysis was performed by The University of Manchester microanalytical laboratory. TGA measurements were carried out by a Seiko SSC/S200 model at a heating rate of 10 °C min^{-1} under nitrogen.

Synthesis of Bis(1,1,5,5-tetramethyl-2-thiobiureto)nickel(II) $[Ni(SON(CNMe_2)_2)_2]$ (1). A solution of dimethylcarbamoyl chloride (1.0 g, 9 mmol) and sodium thiocyanate (0.75 g, 9 mmol) in acetonitrile (25 mL) was heated to reflux with continuous stirring for 1 h, during which time a fine precipitate of sodium chloride formed. To the cooled reaction mixture was added dimethylamine (40% in water) (2.24 mL, 18 mmol) followed by stirring for 30 min and addition of nickel acetate tetrahydrate (1.15 g, 4.5 mmol). The crude product precipitated as a violet powder and was recrystallized from tetrahydrofuran to give suitable crystals for X-ray crystallography. Yield 1.89 g (50%). Mpt: 286 °C. Mass (MS-APCI) (major fragments, m/z): 406 [M^+, $Ni(C_6H_{12}N_3OS)_2$], 174 $[NSO(CNMe_2)_2]$. IR (ν_{max}/cm^{-1}): 1531(b), 1481(s), 1456(b), 1346(s), 1255(b), 1193(b), 1110(b), 1028(s), 908(b), 828(s). Elemental analysis (%): Calc. For $C_{12}H_{24}N_6S_2O_2Ni$: C 35.4; H 5.9; N 20.6; S 15.7; Ni 14.4. Found: C 35.3; H 6.0; N 20.6, S 15.4; Ni 14.1.

Synthesis of Bis(1,1-dimethyl-5,5-diethyl-2-thiobiureto)nickel(II) $[Ni(SON(CNMe_2CNEt_2))_2]$ (2). Complex (**2**) was synthesized by the method described for complex (**1**) using diethylamine. The crude product precipitated as a violet powder and was recrystallized from tetrahydrofuran. Yield 1.54 g (36%). Mpt: 238 °C. Mass (MS-APCI) (major fragments, m/z): 462 [M^+, $Ni(C_8H_{16}N_3OS)_2$], 202 $[NSO(CNMeEt)_2]$. IR (ν_{max}/cm^{-1}): 1529(b), 1481(s), 1388(b), 1351(s), 1256(b), 1198(b), 1115(b), 1032(s), 922(b). Elemental analysis (%): Calc. For $C_{16}H_{32}N_6S_2O_2Ni$: C 41.5; H 6.9; N 18.1; S 13.8; Ni 12.6. Found: C 40.7; H 6.3; N 17.6; S 13.2; Ni 12.2.

Synthesis of Bis(1,1,5,5-tetraethyl-2-thiobiureto)nickel(II) $[Ni(SON(CNEt_2)_2)_2]$ (3). Complex (**3**) was synthesized by the method described for complex (**1**) using diethylcarbamoyl chloride (1.0 g, 7 mmol) and diethylamine (1.5 mL, 14 mmol). The solution was kept overnight at room temperature and gave violet crystals suitable for X-ray crystallography. Yield 1.32 g (35%). Mpt: 140 °C. Mass (MS-APCI) (major fragments, m/z): 518 [M+, $Ni(C_8H_{16}N_3OS)_2$], 258 $[NSO(CNEt)_2]$. IR (vmax/cm-1): 1539(b), 1514(s), 1474(s), 1474(s), 1428(b), 1401(b), 1370(s), 1350(s), 1296(b), 1253(s), 1222(b), 1174(b), 1107(s). Elemental analysis (%): Calc. For $C_{24}H_{48}N_6S_2O_2Ni$: C 46.2; H 7.7; N 16.2; S 12.3; Ni 11.2. Found: C 46.2; H 8.0; N 16.1; S 11.9; Ni 11.9.

Synthesis of Bis(1,1,5,5-tetraisopropyl-2-thiobiureto)nickel(II) $[Ni(SON(CN^iPr_2)_2)_2]$ (4). Complex (**4**) was synthesized by the method described for complex (**1**) using diisopropylcarbamoyl chloride (1.0 g, 6 mmol) and diisopropylamine (1.49 mL, 12 mmol). The solution was kept overnight at room temperature and gave violet crystals suitable for X-ray crystallography. Yield 1.78 g (46%), mpt 177 °C; MS (APCI) major fragments: m/z = [M+]

(17) Barthelemy, E.; Gorochov, O.; McKinzie, H. *Mater. Res. Bull.* **1973**, *8*, 1401.
(18) Pramanik, P.; Bhattacharya, S. *J. Mater. Sci. Lett.* **1987**, *6*, 1105.
(19) Sartale, S. D.; Lokhande, C. D. *Mater. Chem. Phys.* **2001**, *72*, 101.
(20) Lee, H.; Kanai, M.; Kawai, T.; Kawai, S. *Jpn. J. App. Phys.* **1993**, *32*, 2100.
(21) Zhang, L.; Yu, J. C.; Mo, M.; Wu, L.; Li, Q.; Kwang, K. W. *J. Am. Chem. Soc.* **2004**, *126*, 8116.
(22) Yu, S. H.; Yoshimura, M. *Adv. Funct. Mater.* **2002**, *12*, 277.
(23) Nomura, R.; Hayata, H. *Trans. Mater. Res. Soc. Jpn.* **2001**, *26*, 1283.
(24) Alam, N.; Hill, M. S.; Kociok-Kohn, G.; Zeller, M.; Mazar, M.; Molloy, K. C. *Chem. Mater.* **2008**, *20*, 6157.
(25) O'Brien, P.; Waters, J. *Chem. Vap. Deposition* **2006**, *12*, 620.
(26) O'Brien, P.; Park, J. H.; Waters, J. *Thin Solid Films* **2003**, *431−432*, 502.
(27) Musetha, P. L.; Revaprasadu, N.; Malik, M. A.; O'Brien, P. *Mater. Res. Soc. Symp. Proc.* **2005**, *879E*, Z7.4.
(28) Ramasamy, K.; Maneerprakorn, W.; Iqbal, N.; Malik, M. A.; O'Brien, P. *Int. J. Nanosci.*, accepted for publication.
(29) Ramasamy, K.; Malik, M. A.; O'Brien, P.; Raftery, J. *Dalton Trans.* **2010**, *39*, 1460.

631; [Ni($C_{14}H_{28}N_3OS)_2$], [NSO($CN^iPr_2)_2$] 284. IR (ν_{max} /cm^{-1}): 2966(s), 2927(s), 2361(s), 2336(s), 1520(s), 1494(m), 1428(m), 1356(m), 1285(m), 1262(m), 1209(m), 1148. Elemental analysis (%): Calc. For $C_{28}H_{56}N_6S_2O_2Ni$: C, 53.2; H, 8.8; N, 13.3; S, 10.1; Ni, 9.2%. Found: C, 53.2; H, 9.0; N, 13.2; S, 9.9; Ni, 9.0.

Synthesis of Bis(1,1,5,5-tetramethyl-2,4-thiobiureto)nickel(II) [Ni(N(SCNMe$_2$)$_2$)$_2$] (5). A solution of dimethylthiocarbamoyl chloride (1.23 g, 10 mmol) and sodium thiocyanate (0.81 g, 10 mmol) in acetonitrile (25 mL) was heated to reflux with continuous stirring for 1 h, during which time a fine precipitate of sodium chloride formed. To the cooled reaction mixture was added a 40% solution of dimethylamine (1.49 mL, 12 mmol) followed by stirring for 30 min and addition of nickel acetate tetrahydrate (0.76 g, 3 mmol). Crude product was isolated as brown powder. Yield 2.24 g (51%). Mpt: 250 °C. Mass (MS-APCI) (major fragments, m/z): 438 [M^+, Ni($C_6H_{12}N_3S_2)_2$], 190 [N(SCNMe$_2$)$_2$]. IR (ν_{max} /cm^{-1}): 1491(s), 1392(b), 1353(b), 1318(s), 1112(s), 1047(b), 977(b), 909(s). Elemental analysis (%): Calc. For $C_{12}H_{26}N_6S_4Ni$: C 32.6; H 5.8; N 19.0; S 29.0; Ni 13.3. Found: C 32.3; H 6.1; N 18.6; S 28.5; Ni 13.1.

Synthesis of Bis(1,1-dimethyl-5,5-diethyl-2,4-thiobiureto)-nickel(II) [Ni(N(SCNMe$_2$SCNEt$_2$))$_2$] (6). Complex (**6**) was synthesized by the method described for complex (**5**) using diethylamine. The crude product was isolated as brown powder. Diffusion from hexane and dichloromethane gave brown needles suitable for X- crystallography. Yield 1.65 g (35%). Mpt: 191 °C. Mass (MS-APCI) (major fragments, m/z): 465 [M+, Ni($C_8H_{16}N_3S_2)_2$], 218 [N(SCNMeEt)$_2$]. IR (vmax/cm-1): 1484(s), 1417(b), 1371(b), 1346(s), 1325(s), 1263(s), 1231(b), 1126(s), 1076(s). Elemental analysis (%): Calc. For $C_{18}H_{32}N_6S_4Ni$: C 41.2; H 6.8; N 18.0; S 27.4; Ni 12.5. Found: C 40.4; H 6.5; N 17.1; S 26.0; Ni 12.2.

Synthesis of Bis(1,1,5,5-tetraethyl-2,4-thiobiureto)nickel(II) [Ni(N(SCNEt$_2$)$_2$)$_2$] (7). Complex (**7**) was synthesized by the method described for complex (**5**) using diethylthiocarbamoyl chloride (1.0 g, 6 mmol) and diethylamine (0.68 mL, 12 mmol). The solution was kept overnight at room temperature, and brown crystals were obtained suitable for X-ray crystallography. Yield 2.32 g (70%). Mpt: 160 °C. Mass (MS-APCI) (major fragments, m/z): 550 [M+, Ni($C_{12}H_{24}N_3S_2)_2$], 246 [N(SCNEt$_2$)$_2$]. IR (vmax/cm-1): 1484(s), 1425(s), 1404(b), 1376(s), 1332(s), 1247(s), 1126(s), 1071(s), 992(b). Elemental analysis (%): Calc. For $C_{24}H_{48}N_6S_4Ni$: C 43.6; H 7.2; N 15.2; S 23.2; Ni 10.6. Found: C 43.7; H 7.5; N 15.2; S 22.8; Ni 10.2.

X-ray Crystallography. Single-crystal X-ray diffraction data for the compounds were collected using graphite monochromated Mo−Kα radiation (λ = 0.71073 Å) on a Bruker APEX diffractometer. The structures were solved by direct methods and refined by full-matrix least-squares[30] on F^2. All non-H atoms were refined anisotropically. H atoms were included in calculated positions, assigned isotropic thermal parameters, and allowed to ride on their parent carbon atoms. All calculations were carried out using the SHELXTL package.[31] The details for the data collection of the crystals are as follows (**1**): $C_{12}H_{24}N_6O_2S_2Ni$; M = 407.20; violet blocks; orthorhombic; Pnma; a = 13.888(3) Å, b = 6.963(1) Å, c = 18.451(3) Å; V = 1784.3(6) Å^3; Z = 4; D = 1.516 Mg/m^3; T = 100(2) K; reflections collected = 9783, unique reflections = 1984/[R(int) = 0.1005]; R1 = 0.0643 and wR2 = 0.1193 for [I > 2σ(I)]; R1 = 0.0904 and wR2 = 0.1288 for all data; largest diff. peak and hole = 0.745 and −0.659 e.A^{-3}, GOF = 1.160. (**3**): $C_{20}H_{40}N_6O_2S_2Ni$; M = 519.41; violet blocks; orthorhombic; Pbca; a = 10.689(2) Å, b = 18.763(3) Å, c = 25.788(4) Å; V = 5172(2) Å^3; Z = 8; D = 1.334 Mg/m^3; T = 100(2) K; reflections collected = 38878, unique reflections = 5311/ [R(int) = 0.0725]; R1 = 0.0295 and wR2 = 0.0646 for [I > 2σ(I)]; R1 = 0.0420 and wR2 = 0.0679 for all data; largest diff. peak and hole = 0.461 and −0.242 e.A^{-3}, GOF = 0.966. (**4**) $C_{28}H_{56}N_6O_2S_2Ni$; M = 631.62; violet plate; monoclinic; $P2_1/c$; a = 21.787 Å, b = 13.777 Å, c = 11.925 Å; β = 90.99°; V = 3578.9 Å^3; Z = 4; D = 1.172 Mg/m^3; T = 100(2) K; reflections collected = 16324, unique reflections = 6984/[R(int) = 0.1107]; R1 = 0.0781 and wR2 = 0.1718 for [I > 2σ(I)]; R1 = 0.1877 and wR2 = 0.2183 for all data; largest diff. peak and hole = 1.379 and −0.994 e.A^{-3}, GOF = 0.939. (**6**): $C_{16}H_{32}N_6S_4Ni$; M = 495.43; brown needles; monoclinic; $P2_1/c$; a = 8.143(2) Å, b = 17.389(4) Å, c = 8.304(2) Å; β = 110.001(4)°; V = 1104.9(4) Å^3; Z = 2; D = 1.489 Mg/m^3; T = 100(2) K; reflections collected = 9159, unique reflections = 2436/[R(int) = 0.1024]; R1 = 0.0586 and wR2 = 0.0755 for [I > 2σ(I)]; R1 = 0.1060 and wR2 = 0.0853 for all data; largest diff. peak and hole = 0.718 and −0.480 e.A^{-3}, GOF = 0.915. (**7**): $C_{20}H_{40}N_6S_4Ni$; M = 551.53; brown plate; triclinic; P-1; a = 9.494(2) Å, b = 11.456(2) Å, c = 13.758(2) Å; α = 89.628(3)°, β = 89.726(3)°, γ = 67.548(3)° V = 1382.9(4) Å^3; Z = 2; D = 1.325 Mg/m^3; T = 100(2) K; reflections collected = 8092, unique reflections = 5529/[R(int) = 0.0221]; R1 = 0.0477 and wR2 = 0.0991 for [I > 2σ(I)]; R1 = 0.0651 and wR2 = 0.1037 for all data; largest diff. peak and hole = 0.553 and −0.326 e.A^{-3}, GOF = 1.112. CCDC reference numbers: 715967, 715966, 715960, 783952, and 715963.

Deposition of Films by AACVD. In a typical deposition, 0.20 g of the precursor was dissolved in 20 mL of tetrahydrofuran in a two-necked 100 mL round-bottom flask with a gas inlet that allowed the carrier gas (argon) to pass into the solution to aid the transport of the aerosol. This flask was connected to the reactor tube by a piece of reinforced tubing. The argon flow rate was controlled by a Platon flow gauge. Seven glass substrates (approximately 2 × 2 cm) were placed inside the reactor tube, which is placed in a CARBOLITE furnace. The precursor solution in a round-bottom flask was kept in a water bath above the piezoelectric modulator of a PIFCO ultrasonic humidifier (Model No. 1077). The aerosol droplets of the precursor thus generated were transferred into the hot wall zone of the reactor by carrier gas. Both the solvent and the precursor were evaporated, and the precursor vapor reached the heated substrate surface where thermally induced reactions and film deposition took place.

Characterization of Thin Films. X-ray diffraction studies were performed on a Bruker AXS D8 diffractometer using Cu−Kα radiation. The samples were mounted flat and scanned between 20 and 80° in a step size of 0.05 with a count rate of 9 s. Films were carbon coated using Edward's E306A coating system before carrying out SEM and EDX analyses. SEM analysis was performed using a Philips XL 30FEG, and EDX was carried out using a DX4 instrument. TEM analysis was performed using a cm200 instrument. High resolution transmission electron microscopy (HRTEM) was performed using a Tecnai F30 FEG TEM instrument, operating at 300 kV; all samples were deposited over carbon coated copper grids. Selected area electron diffraction (SAED) was performed using a Phillips CM200 microscope at an accelerating voltage of 200 kV.

Results and Discussion

The series of symmetrical and unsymmetrical nickel(II) complexes of 1,1,5,5-tetraalkyl-2-thiobiuret (alkyl = methyl, [Ni(SON(CNMe$_2$)$_2$)$_2$] (**1**); methyl, ethyl, [Ni(SON(CNMe$_2$-CNEt$_2$))$_2$] (**2**); ethyl, [Ni(SON(CNEt$_2$)$_2$)$_2$] (**3**); isopropyl [Ni(SON($CN^iPr_2)_2$)$_2$] (**4**) and 1,1,5,5-tetraalkyl-2,4-dithiobiuret

(30) Sheldrick, G. M. SHELXS-97 and SHELXL-97; University of Göttingen: Germany, 1997.
(31) Bruker. SHELXTL Version 6.12; Bruker AXS Inc.: Madison, Wisconsin, USA, 2001.

Scheme 1. Schematic Representation of the Synthesis of Ligand and Complexes

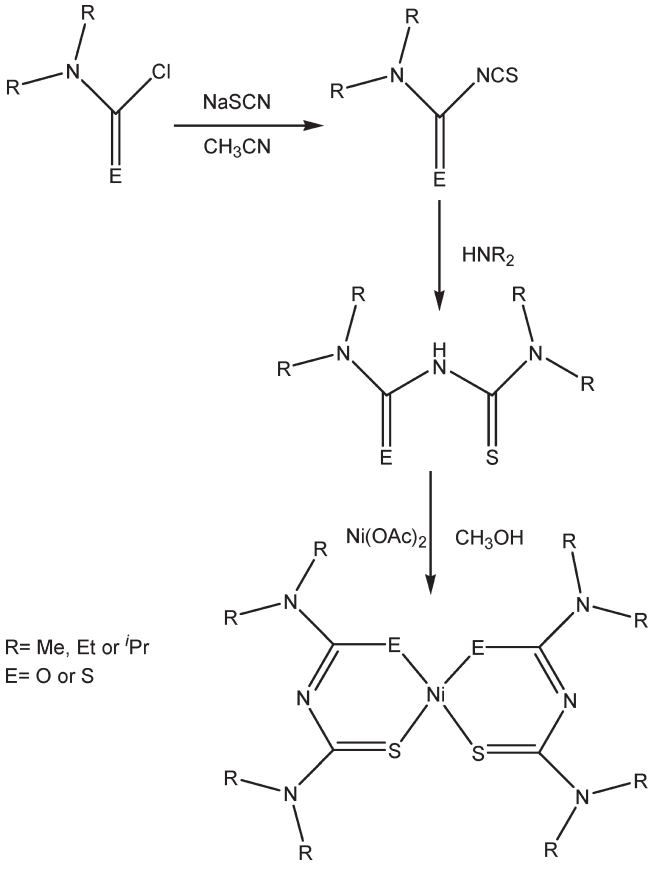

(alkyl = methyl, $[Ni(N(SCNMe_2)_2)_2]$ (**5**); methyl, ethyl $[Ni(N(SCNMe_2SCNEt_2))_2]$ (**6**); ethyl $[Ni(N(SCNEt_2)_2)_2]$ (**7**) were synthesized by the reaction of excess dialkylamine with *in situ* generated dialkylcarbamoylthiocyanate in acetonitrile.[29] A schematic representation for the synthesis of the complexes is shown in Scheme 1. All the complexes are air and moisture stable. Complexes **1**−**4**, **6**, and **7** are soluble in most of the nonpolar solvents. Complex (**5**) was seemingly insoluble in all common solvents which make the complex unsuitable for AACVD experiments.

X-ray Single Crystal Structure of $[Ni(SON(CNMe_2)_2)_2]$ (1). The X-ray single crystal structure of $[Ni(SON(CNMe_2)_2)_2]$ (**1**) shows the nickel(II) ion as square planar with an S_2O_2 donor set (Figure 1a). The sulfur and oxygen atoms are mutually *cis*. Both thiobiuret ligands of each unit are chelating to form two six membered rings (NC_2OS-Ni). The crystal lattice shows the presence of monomeric independent units, which are separated by normal van der Waals distances. The average N−C−O and N−C−S angles are 129.8(4) and 127.8(3)° respectively. In both ligands, the pattern of bond distances indicates that the formal negative charge is predominately localized on the S atom. The relatively long C−S and short C−O average distances of 1.751(4) and 1.262(6) Å are consistent with predominantly single and double bond character, respectively. This bond localization is also reflected in the average C−N bond distances to the central N atom: 1.327(5) Å in the (iso)thiourea group and 1.346(6) Å in the urea group. The urea C(4)−N(2) bond within the

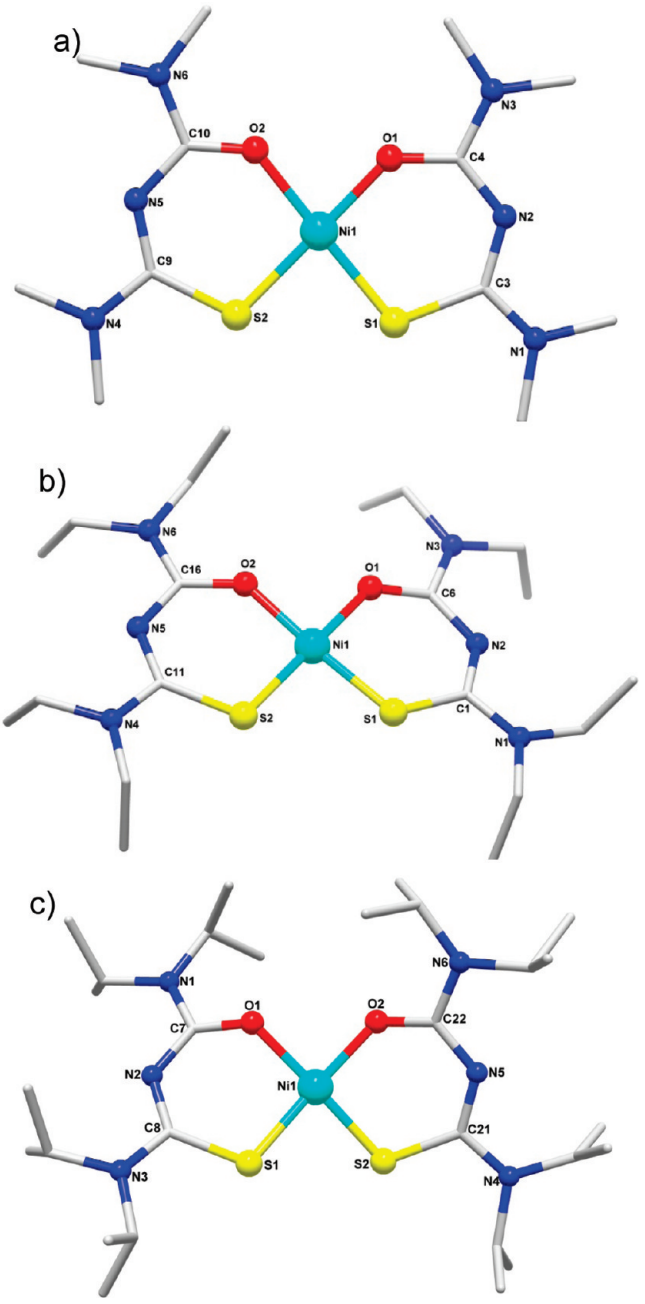

Figure 1. (a) X-ray structure of (**1**). Selected bond lengths (Å) and bond angles (°): Ni1−O1 1.838(4), Ni1−S1 2.140(2), S1−C3 1.758(6), O1−C4 1.266(8); O1−Ni1−O2 83.89(2), O2−Ni1−S1 94.980(2). (b) X-ray structure of (**3**). Selected bond lengths (Å) and bond angles (°): Ni1−O1 1.872(1), Ni1−S1 2.136(6), S1−C1 1.744(2), O1−C6 1.267(2); O1−Ni1−O2 83.76(5), O1−Ni1−S1 94.520(4). (c) X-ray structure of (**4**). Selected bond lengths (Å) and bond angles (°): Ni1−O1 1.882(2), Ni1−S1 2.132(1), S1−C8 1.760(4), O1−C7 1.273(4); O1−Ni1−S2 168.81(9), O2−Ni1−S2 93.790(8). Hydrogen atoms on alkyl groups removed for clarity.

chelate ring is substantially shorter than the exocyclic C−NMe_2 bond 1.368(8) Å, but the thiourea C(3)−N(2) bond 1.334(7) Å in the coordinating ring is somewhat larger than the exocyclic C-NMe_2 bond 1.316(7) Å. The average metal to sulfur bond (2.139(1) Å) is longer than the metal to oxygen bond (1.855(3)). The bond angles of O(1)−Ni(1)−S(1) and O(2)−Ni(1)−S(2) are 94.98(2) and 95.59(1), respectively, which are slightly larger than perfect square planar angle. Selected bond angles and bond lengths are given in the caption

to Figure 1a. Structure refinement is listed in the Experimental Section.

X-ray Single Crystal Structure of [Ni(SON(CNEt$_2$)$_2$)$_2$] (3). The X-ray single crystal structure of (**3**) shows nickel(II) ion is square planar with an S_2O_2 donor set (Figure 1b). The sulfur and oxygen atoms are mutually *cis* at the edges of a square as observed in complex (**1**). The presence of the ethyl group leads to some deviation from planarity. The average N−C−O and N−C−S angles are 129.2(1) and 129.6(1)° respectively. In both ligands, the pattern of bond distances indicates that the formal negative charge is predominately localized on the S atom. The relatively long C−S and short C−O average bond lengths of 1.745(1) and 1.273(1) Å are consistent with mostly single and double bond character as observed for complex (**1**), and the C−S bond is not significantly different to that observed in the crystal structure of complex (**1**). This bond localization is also reflected in the average C−N bond distances to the central N atom: 1.323(1) Å in the (iso)thiourea group and 1.348(1) Å in the urea group, which are also similar to those bond lengths observed for complex (**1**). The average metal to sulfur bond (2.138(4) Å) is longer than the metal to oxygen bond (1.8595(8)). The bond angles of O(1)−Ni(1)−S(1) and O(2)-Ni(1)−S(2) are 94.52(2) and 95.26(1), respectively, which are slightly larger than perfect square planar angle. Selected bond angles and bond lengths are given in the caption to Figure 1b. Structure refinement is listed in the Experimental Section.

X-ray Single Crystal Structure of [Ni(SON(CN^{i}Pr$_2$)$_2$)$_2$] (4). The X-ray single crystal structure of [Ni(SON(CN^{i}Pr$_2$)$_2$)$_2$] (**4**) shows nickel as square planar with a S_2O_2 donor set (Figure 1c). The sulfur and oxygen atoms are *cis*. However, both thiobiurete ligands show significant deviation from planarity due to twisting about the central N atom; the average N−C−O and N−C−S angles are 128.2(2) and 125.9(2)° respectively. In both ligands, the pattern of bond distances indicates that the formal negative charge is predominately localized on the S atom. The relatively long C−S and short C−O average bond lengths of 1.750(3) and 1.272(3) Å are consistent with predominantly single and double bond character, respectively. This bond localization is also reflected in the average C−N bond distances to the central N atom: 1.324(4) Å in the (iso)thiourea group and 1.346(3) Å in the urea group. One of the isopropyl groups in the ligand is disordered over two conformations in the ratio of 62:38. Selected bond angles and bond lengths are given in the caption to Figure 1c. Structure refinement is listed in the Experimental Section. The effect of different alkyl groups on the ligand geometries in complexes (**1**), (**3**), (**4**) is insignificant. However, there does seem to be a slight shortening of the Ni−S bond lengths, and lengthening of the Ni−O bond lengths in the series of complexes (**1**), (**3**) and (**4**), with the alkyl group changing from Me to ^{i}Pr.

X-ray Single Crystal Structure of [Ni(N(SCNMe$_2$-SCNEt$_2$))$_2$] (6). The X-ray single crystal structure of (**6**) shows nickel ion is in a similar square planar environment to (**1**), (**3**) and (**4**) with an S_4 donor set. The NiS_2C_2N rings adopt a slightly distorted chair conformation with dimethyl groups that are mutually *trans* (Figure 2a). The average

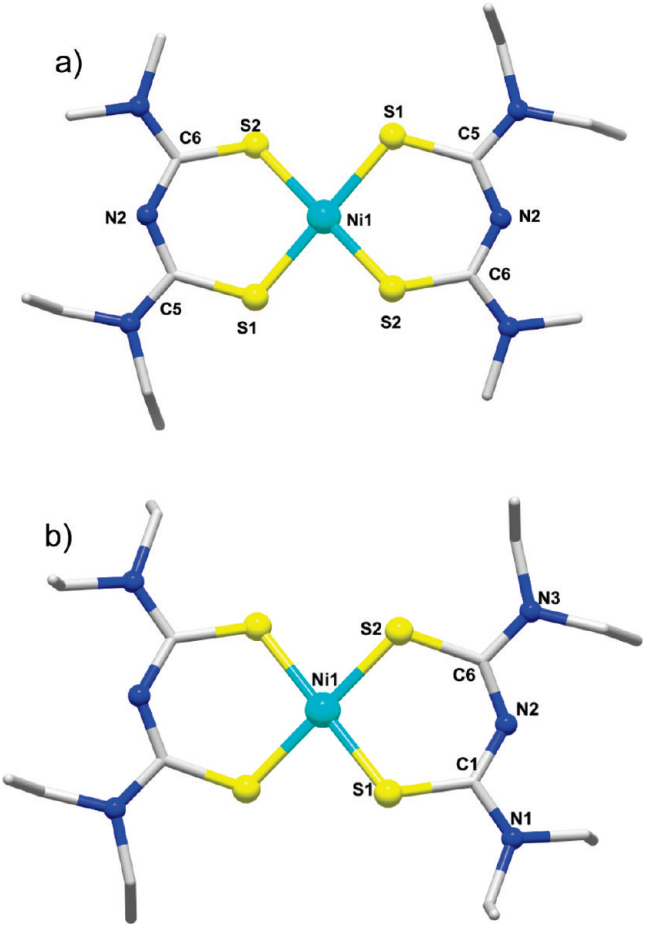

Figure 2. (a) X-ray structure of (**6**). Selected bond lengths (Å) and bond angles (°): Ni1−S1 2.173(1), C6−S2 1.740(4), C5−S1 1.749(4), C6−N2 1.329(5); S1−Ni1−S2 96.51(4), N2−C5−S1 115.70(3). (b) X-ray structure of (**7**). Selected bond lengths (Å) and bond angles (°): Ni1−S1 2.164(1), C6−S2 1.740(3), C1−S1 1.741(3), C6−N2 1.332(4); S2−Ni1−S1 95.65(3), N2−C1−S1 129.40(3). Hydrogen atoms on alkyl groups removed for clarity.

N−C−S angle is 129.0(2)° which is consistent with complexes (**1**), (**3**) and (**4**). In both ligands, the pattern of bond distances indicates that the formal negative charge is delocalized over the NiS_2C_2N rings. The relatively long C(5)−S(1) and C(6)−S(2) bond lengths of 1.749(4) and 1.740(4) Å are consistent with mostly single bond character. The thiourea average C−N (1.329(4) Å) bonds within the chelate ring are substantially shorter than the exocyclic C−NMe$_2$ (1.349(4) Å) bonds. The average metal to sulfur bond (2.178(1) Å) is somewhat longer than observed for complexes (**1**) (2.139(1) Å) and (**3**) (2.138(4) Å).

X-ray Single Crystal Structure of [Ni(N(SCNEt$_2$)$_2$)$_2$] (7). The X-ray single crystal structure of (**7**) shows the nickel ion is in a similar square planar environment to (**6**) with an S_4 donor set. The NiS_2C_2N rings adopt a nearly perfect chair conformation. The average N−C−S angle is 129.4(2)° which is consistent with complex (**6**). In both ligands, the pattern of bond distances indicates that the formal negative charge is delocalized over the NiS_2C_2N rings. The relatively long C(1)−S(1) and C(6)−S(2) bond lengths of 1.741(3) and 1.740(3) Å are consistent with mostly single bond character as observed for complex (**1**). The thiourea C−N bonds within the chelate ring are

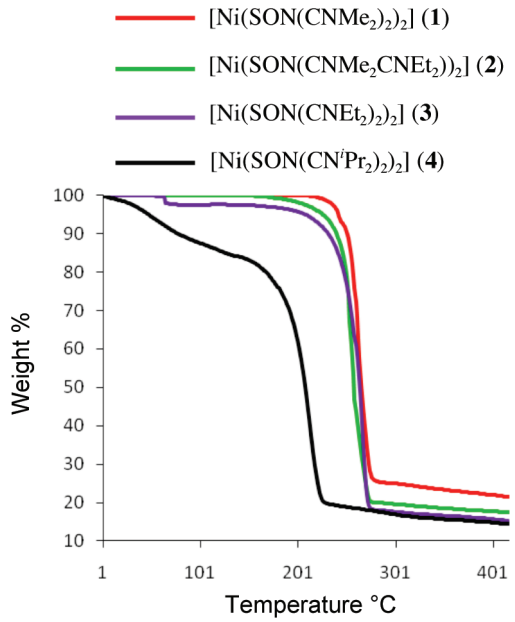

Figure 3. TGA of complexes [Ni(SON(CNMe$_2$)$_2$)$_2$] (**1**), [Ni(SON(CNMe$_2$CNEt$_2$))$_2$] (**2**), [Ni(SON(CNEt$_2$)$_2$)$_2$] (**3**), and [Ni(SON(CN^{i}Pr$_2$)$_2$)$_2$] (**4**).

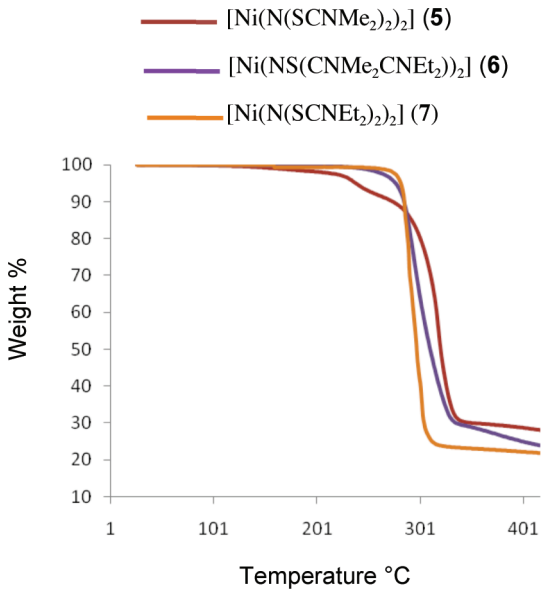

Figure 4. TGA of complexes [Ni(N(SCNMe$_2$)$_2$)$_2$] (**5**), [Ni(N(SCNMe$_2$SCNEt$_2$))$_2$] (**6**), and [Ni(N(SCNEt$_2$)$_2$)$_2$] (**7**).

significantly shorter than the exocyclic C−NEt$_2$ (1.332(2) Å versus 1.349(2) Å) bonds as like (**6**). The average metal to sulfur bond (2.163(5) Å) is somewhat longer than observed for complex (**1**) (2.139(1) Å), (**3**) (2.138(4) Å), and (**4**) ((2.129(8) Å) but shorter than the bond distance observed for complex (**6**) (2.178(1) Å). The crystal lattice shows the presence of two similar monomeric independent units. Selected bond angles and bond lengths are given in the caption to Figure 2(b). Structure refinement is listed in the Experimental Section.

The above structural analyses show that all five thio and dithiobiuret complexes are monomers with nickel(II) in a square planar geometry. In complexes (**1**), (**3**), and (**4**) the thiobiuret ligands are coordinated through the S_2O_2 donor set with the two sulfur and two oxygen atoms each mutually *cis*. The change in the alkyl group from methyl to isopropyl shortens the metal to sulfur bond in the thiobiuret complexes; in the dithiobiuret complexes, the average metal to sulfur bond shortens on changing the alkyl groups from mixed methyl and ethyl in (**6**) to all ethyl in (**7**). Overall, the metal to sulfur bond is shorter in the thiobiuret complexes than the dithiobiuret complexes.

Thermogravimetric Analysis of Thiobiuret Complexes (1)-(4). Thermogravimetric analysis (TGA) provides information about the decomposition processes and volatility of the precursors under study. TGA of the complexes [Ni(SON(CNMe$_2$)$_2$)$_2$] (**1**), [Ni(SON(CNMe$_2$CNEt$_2$))$_2$] (**2**), [Ni(SON(CNEt$_2$)$_2$)$_2$] (**3**), and [Ni(SON(CN^{i}Pr$_2$)$_2$)$_2$] (**4**) indicated a single step decomposition with a rapid weight loss between 255 and 319 °C, 299−316 °C, 280−313 °C, and 234−255 °C, respectively (Figure 3). The solid decomposition residue amounts to 24.0% for (**1**), which is in agreement with the calculated value of 22.3% for NiS. Similarly the observed final residues amount to 20.3% for (**2**) and 18.0% for (**3**) which are in good agreement with the calculated values of NiS for 19.6% and 17.4%, respectively, whereas the final residue observed for complex (**4**) of 21.4% is close to the calculated value of 19.4% for nickel disulfide.

Thermogravimetric Analysis of Dithiobiuret Complexes (5)-(7). The complexes [Ni(N(SCNMe$_2$)$_2$)$_2$] (**5**), [Ni(N(SCNMe$_2$SCNEt$_2$))$_2$] (**6**), and [Ni(N(SCNEt$_2$)$_2$)$_2$] (**7**) decompose in a single step with a loss of mass at a temperature between 257−332 °C, 278−326 °C, and 269−309 °C, respectively (Figure 4). The observed final residue of 30.3% for (**5**) is close to the calculated value of 28.0 for nickel disulfide. The final residue of 28.3% for (**6**) is closer to the calculated value of 26.3 for nickel disulfide. Similarly the final residue obtained in decomposition of complex (**7**) is 23.2% with good agreement the calculated value of 22.2% for nickel disulfide. The above thermogravimetric analysis shows that thiobiuret complexes (**1**), (**2**), and (**3**) which have a sulfur to metal ratio of 2 decompose to NiS, in contrast, the mass of the final residue obtained from complex (**4**) is closer to that for NiS_2. The dithiobiuret complexes (**5**), (**6**), and (**7**) with a sulfur to metal ratio of 4 decomposes in a single step to NiS_2. This observation gives an idea that complexes with a higher sulfur to metal ratio decompose to sulfur rich nickel sulfide phases.

Deposition of Nickel Sulfide Thin Films from [Ni(SON(CNMe$_2$)$_2$)$_2$] (1). The XRD pattern of as deposited films at 320−440 °C (Figure 5) shows the deposition of Ni_7S_6 nickel sulfide, indexed in which all cases as the orthorhombic phase of Ni_7S_6 (ICDD: 024-1021). The X-ray diffractions pattern of films deposited at 320 °C showed amorphous material with weak diffraction peaks. At 360 °C sharper peaks for (044) and (200) of Ni_7S_6 were obtained. Films deposited at 400 and 440 °C gave intense of (121), (131), and (056) reflections. The major peaks (042), (121), (131), (312), (062), and (056) can be assigned to orthorhombic Ni_7S_6.

The SEM images of the films (Figure 6) show that the morphology of the nickel sulfide is dependent on the growth temperature and growth period. Films deposited

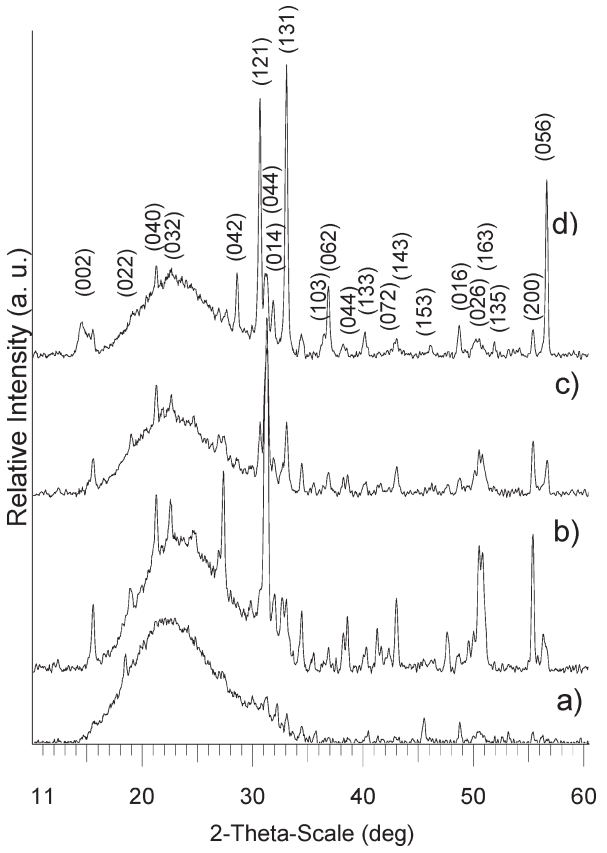

Figure 5. XRD pattern of nickel sulfide thin films deposited from $[Ni(SON(CNMe_2)_2)_2]$ (**1**) on glass at (a) 320 °C, (b) 360 °C, (c) 400 °C, and (d) 440 °C.

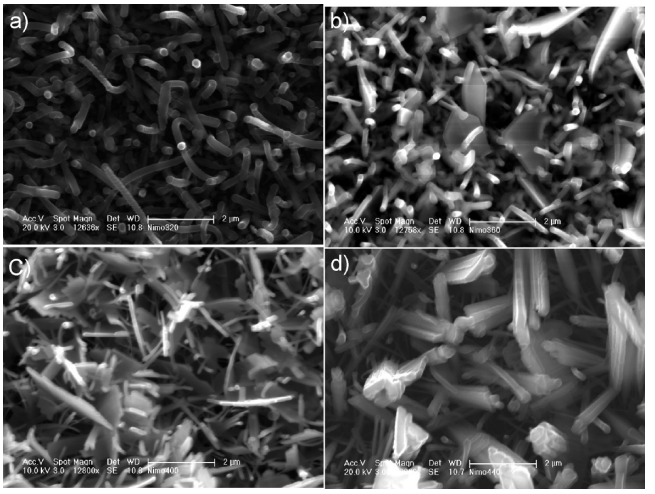

Figure 6. SEM images of films deposited from $[Ni(SON(CNMe_2)_2)_2]$ (**1**) on glass at (a) 320 °C, (b) 360 °C, (c) 400 °C, and (d) 440 °C.

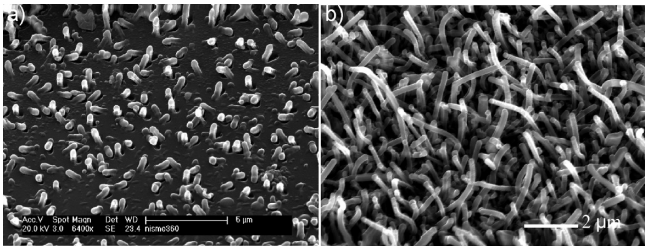

Figure 7. Tilted SEM (45°) images of films deposited from [Ni(SON-$(CNMe_2)_2)_2$] (**1**) on glass at 320 °C (a) 5 min and (b) 60 min.

at 320 °C consist of wirelike crystallites with rounded tip. The average width of wires was 200 ± 20 nm. A tilted SEM (45°) image showed an average length of 2 ± 0.1 μm (Figure 7(a)). In order to identify the growth pattern of tipped wires, the deposition was stopped in 5 min and the SEM image of corresponding films showed initial formation of spherical crystallites (Figure 7(b)). The films deposited at 360 and 400 °C consist of wires and plates, whereas at 440 °C the morphology appears to be pillars composed of wires. EDX analysis of the films confirms the composition as Ni:S in ratios of 55:45 (320 and 360 °C), 54:46 (400 °C), and 53:47 (440 °C).

The TEM images of scratched crystallites from the films grown at 440 °C show the width of nanobelts ranging from *ca.* 20 to 30 nm as shown in Figure 8 (a). HRTEM images of the nanobelts (Figure 8(c)) show the lattice fringes with a *d*-spacing of 1.62 Å corresponding to (056) reflection of orthorhombic Ni_7S_6. The SAED pattern in Figure 8(d) shows the single crystalline nature of nanoplates. The diffraction spot can be indexed to the (121) plane of the orthorhombic phase.

Deposition of Nickel Sulfide Thin Films from [Ni(SON-$(CNMe_2CNEt_2))_2$] (2). Nickel sulfide film deposition was achieved in the temperature range between 320 and 440 °C. At 320 and 360 °C black, adherent but nonuniform films were deposited, whereas at 400 and 440 °C black, uniform films were obtained. The X-ray diffraction (XRD) pattern of as deposited films at 320−440 °C from complex (**2**) shows the mixture of hexagonal $Ni_{17}S_{18}$ (ICDD: 070-2306) and orthorhombic Ni_7S_6 phases (ICDD: 024-1021) (see the Supporting Information). The XRD pattern obtained from the films deposited at 320 °C shows less intense peaks with almost the same ratio of orthorhombic and hexagonal phases. At 360 °C the hexagonal phase was observed predominantly with high intense peaks of (042), (004), (026), (163), and (242). At 400 °C almost the same ratio of both phases was obtained, whereas the XRD pattern of films deposited at 440 °C shows the deposition of higher amounts of orthorhombic Ni_7S_6 with major diffraction peaks of (121), (031), (062), and (056) planes. The transformation of the sulfur rich hexagonal $Ni_{17}S_{18}$ phase to the sulfur deficient orthorhombic N_7S_6 phase when increasing the deposition temperature could be explained by the loss of sulfur at higher deposition temperature.

The SEM images of nickel sulfide thin films deposited from complex (**2**) are shown in Figure 9. At 320 °C almost uniform wires were deposited with an average width of 200 ± 20 nm and several micrometers in length. At 360 °C platelike crystallites with an average thickness of 200 ± 15 nm were deposited, and at 400 °C wires with a rough surface were obtained. The average width of these wires was 300 ± 20 nm, with a several micrometer length. The deposition at 440 °C produced the crystallites in the shape of plates stacked on the top of each other. The average thickness of plates could be measured as 150 ± 10 nm. The morphology of films deposited from complex (**2**) is entirely different from the morphology of films deposited from

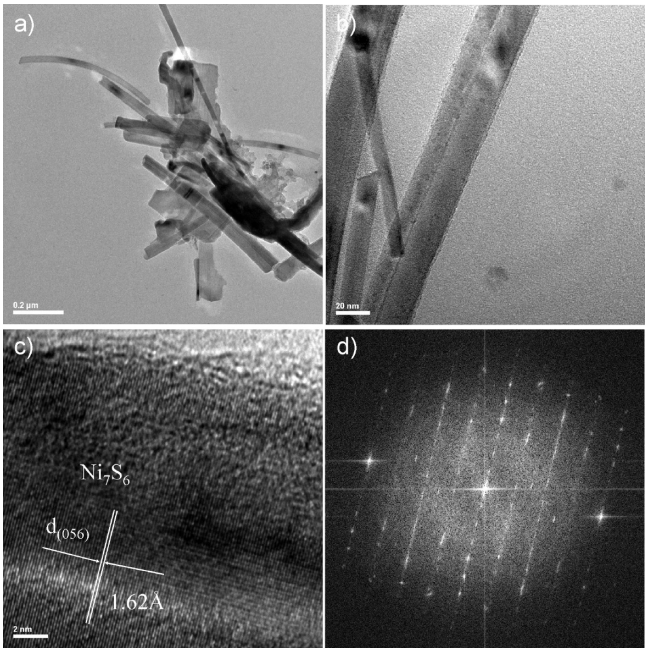

Figure 8. (a) and (b) TEM images, (c) HRTEM images, and (d) SAED pattern of nickel sulfide films deposited from [Ni(SON($CNMe_2$)$_2$)$_2$] (**1**) on glass at 440 °C.

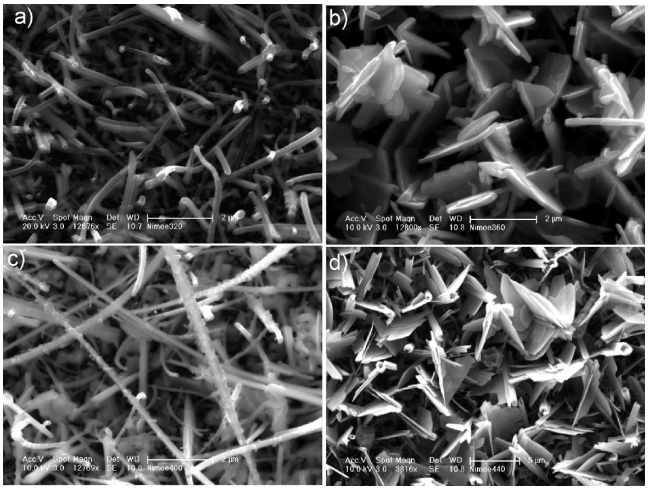

Figure 9. SEM images of films deposited from [Ni(SON($CNMe_2$-$CNEt_2$))$_2$] (**2**) on glass at (a) 320 °C, (b) 360 °C, (c) 400 °C, and (d) 440 °C.

complex (**1**). This observation may be explained by the presence of the diethyl group on complex (**2**) altering the decomposition of complex inside the CVD reactor. The composition of films deposited from complex (**2**) at different deposition temperatures was analyzed by EDX as Ni:S: 52.6:47.4 (320 °C), 53.6:46.4 (360 °C), 54.6:45.4 (400 °C), and 54.3:45.7 (440 °C).

The TEM images show the scratched crystallites from the films grown at 400 °C consist of nanobelts with an average width of 15 ± 2 nm (Figure 10(a)). HRTEM images of the nanobelts (Figure 10(d)) show the lattice fringes with a *d*-spacing of 1.62 Å corresponding to the (056) reflection of orthorhombic Ni_7S_6.

Deposition of Nickel Sulfide Thin Films from [Ni(SON-($CNEt_2$)$_2$)$_2$] (3). Thin films of nickel sulfide have been deposited from complex (**3**) in the temperature range of

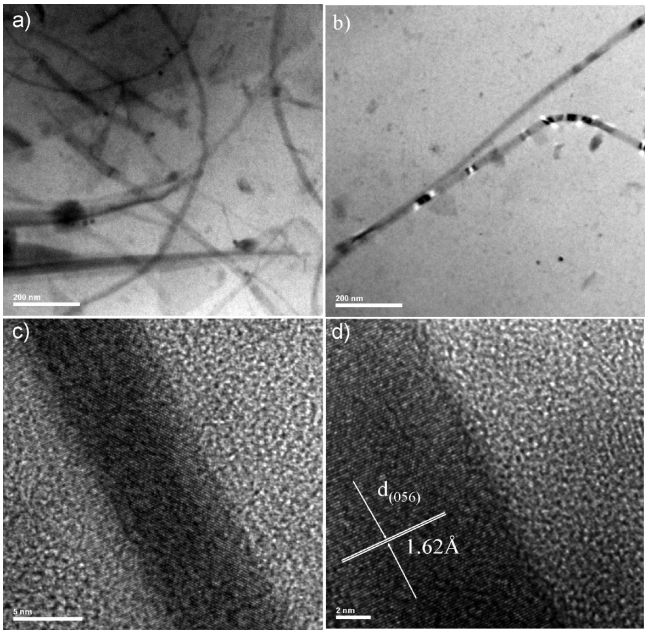

Figure 10. (a) and (b) TEM images (c) and (d) HRTEM images of nickel sulfide deposited from [Ni(SON($CNMe_2CNEt_2$))$_2$] (**2**) on glass at 440 °C.

320 to 440 °C on glass substrate. Black, adherent, uniform films were deposited at all temperatures. The X-ray diffraction (XRD) pattern of as deposited films at 320−440 °C from complex (**3**) shows a mixture of hexagonal $Ni_{17}S_{18}$ (ICDD: 070-2306) and orthorhombic Ni_7S_6 (ICDD: 024-1021) (see the Supporting Information). The XRD pattern obtained from the films deposited at 320 °C shows reflections for the hexagonal $Ni_{17}S_{18}$ phases. At 360 and 400 °C almost the same intensity of reflections from both phases is obtained, whereas the XRD pattern of films deposited at 440 °C shows sharp intense peaks for (042), (004), and (163) planes of orthorhombic Ni_7S_6.

The SEM images of nickel sulfide thin films deposited from complex (**3**) are shown in Figure 11. At 320 °C irregular crystallites deposited with an average size of 300 ± 20 nm, whereas at 360 and 400 °C cross-linked platelike crystallites with an average thickness of 300 ± 35 nm and 350 ± 25 nm were obtained. Films deposited at 440 °C showed clusters composed of platelike crystallites. The average thickness of plates could be measured as 100 ± 10 nm. The morphology of films deposited from complex (**3**) was different from the morphology of films deposited from complex (**1**) or (**2**). The compositions of films deposited from complex (**3**) were confirmed by EDX analysis as Ni:S ratios: 52.1:47.9 (320 °C), 53.7:46.3 (360 °C), 54.5:45.5 (400 °C), and 56.0:44.0 (440 °C).

The TEM images show the scratched crystallites from the films grown at 440 °C consist of nanobelts with an average width size of 415 ± 10 nm (Figure 12(a)). HRTEM images of the nanobelts (Figure 12(c)) show the lattice fringes with a *d*-spacing of 2.44 Å corresponding to (131) reflection of orthorhombic Ni_7S_6. FFT image in Figure 12(d) confirms the single crystalline nature of crystallites.

Deposition of Nickel Sulfide Thin Films from [Ni(SON-(CN^iPr_2)$_2$)$_2$] (4). Film deposition was carried out at substrate temperature between 320 to 400 °C with an argon

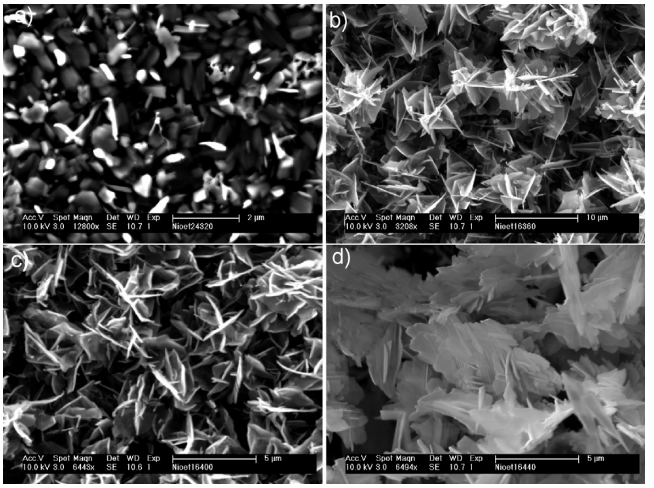

Figure 11. SEM images of films deposited from $[Ni(SON(CNEt_2)_2)_2]$ (**3**) on glass at (a) 320 °C, (b) 360 °C, (c) 400 °C, and (d) 440 °C.

flow rate of 160 sccm. No deposition was obtained below 320 °C. Black, adherent films were deposited at 320 and 360 °C, but uniform black films were deposited at 400 °C.

The XRD pattern of as deposited films at 320−400 °C (Figure 13) show the formation of Ni_9S_8 phase nickel sulfide indexed as the orthorhombic phase of Ni_9S_8 (ICDD: 04-007-0778). No significant XRD peaks from impurities were observed. The X-ray diffractions pattern of films deposited at 320 °C show sharper peaks than those deposited at 360 or 400 °C. The major peaks (310), (113), (023), (312), (060), and (135) are assigned to orthorhombic Ni_9S_8.

The SEM images of the films (Figure 14) show that the morphology of the nickel sulfide is dependent on the growth temperature. Films deposited at 320 and 360 °C consist of flowerlike crystallites with an average size of 4 ± 0.2 μm and 15 ± 1 μm, respectively, where as film deposited at 400 °C showed branched structures. EDX analysis of the films shows the composition as a Ni:S ratio: 49.0:51.0 (320 °C), 50.2:49.8 (360 °C), and 52.4:47.6 (400 °C).

The TEM images show the scratched crystallites from the film grown at 400 °C consist of nanobelts with a size ranging from *ca.* 200 to 300 nm (Figure 15(a)). HRTEM images of the nanobelts (Figure 15(b) and (c)) show the lattice fringes with a *d*-spacing 2.99 nm corresponding to a (310) reflection of orthorhombic Ni_9S_8. The FFT pattern in Figure 15(d) shows the single crystalline nature of nanoplates.

Deposition of Nickel Sulfide Thin Films from $[Ni(N(SCNMe_2SCNEt_2))_2]$ (6). Film deposition was carried out at a substrate temperature between 360 to 480 °C with an argon flow rate of 160 sccm on a glass substrate using complex (**6**). No deposition was obtained below 360 °C and above 480 °C. Black, adherent, uniform films were deposited at all temperatures.

The X-ray diffraction (XRD) pattern (Figure 16) of as deposited films at 360−480 °C from complex (**6**) shows that films deposited at 360 and 400 °C give NiAs hexagonal type $NiS_{1.03}$ phase with major diffraction peaks for (100), (002), (101), (102), and (110) planes

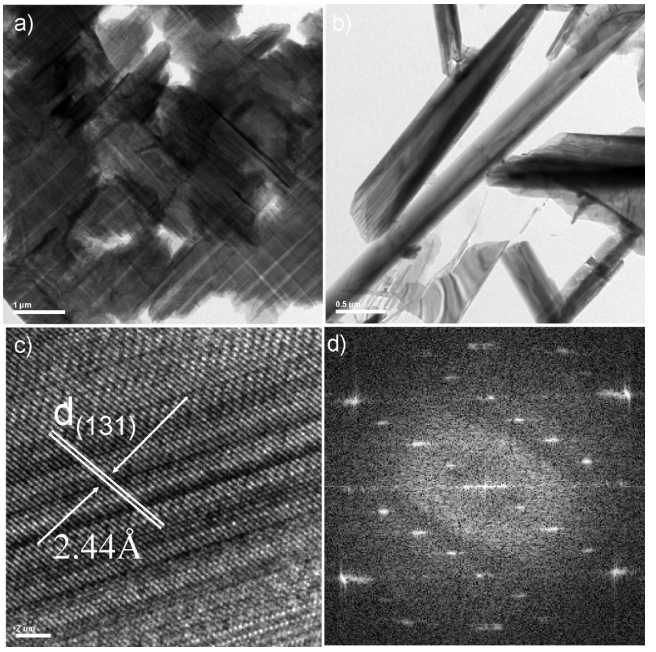

Figure 12. a) and b) TEM images (c) HRTEM images (d) FFT pattern of nickel sulfide films deposited from $[Ni(SON(CNEt_2)_2)_2]$ (**3**) on glass at 440 °C.

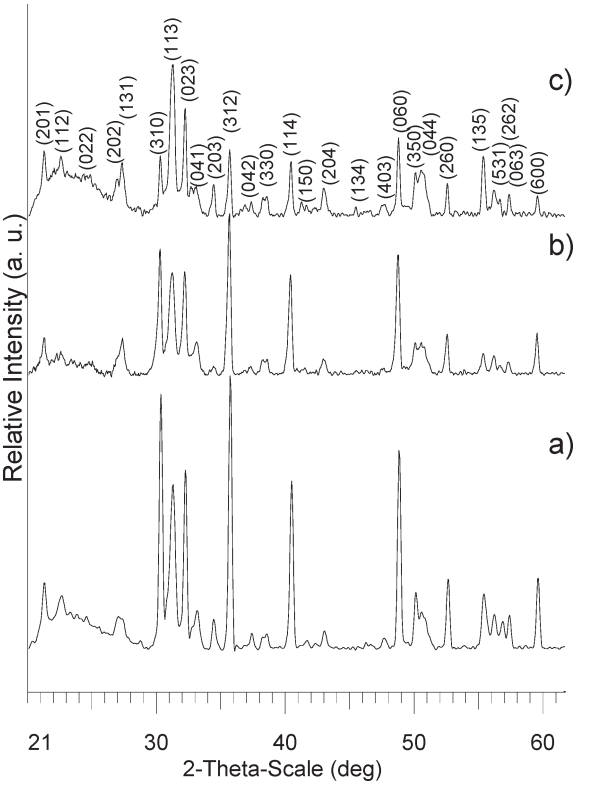

Figure 13. XRD pattern of NiS films deposited from $[Ni(SON(CN^iPr_2)_2)_2]$ (**4**) on glass at (a) 320 °C, (b) 360 °C, and (c) 400 °C.

(ICDD: 002-1273). The XRD pattern for films deposited at 440 and 480 °C shows peaks corresponding to hexagonal $NiS_{1.03}$ and also the orthorhombic Ni_7S_6 phase (ICDD: 024-1021) for (121), (103), (016), and (200) planes. The deposition of the sulfur deficient Ni_7S_6 phase at higher temperatures could be related to the volatility of sulfur at these temperatures.

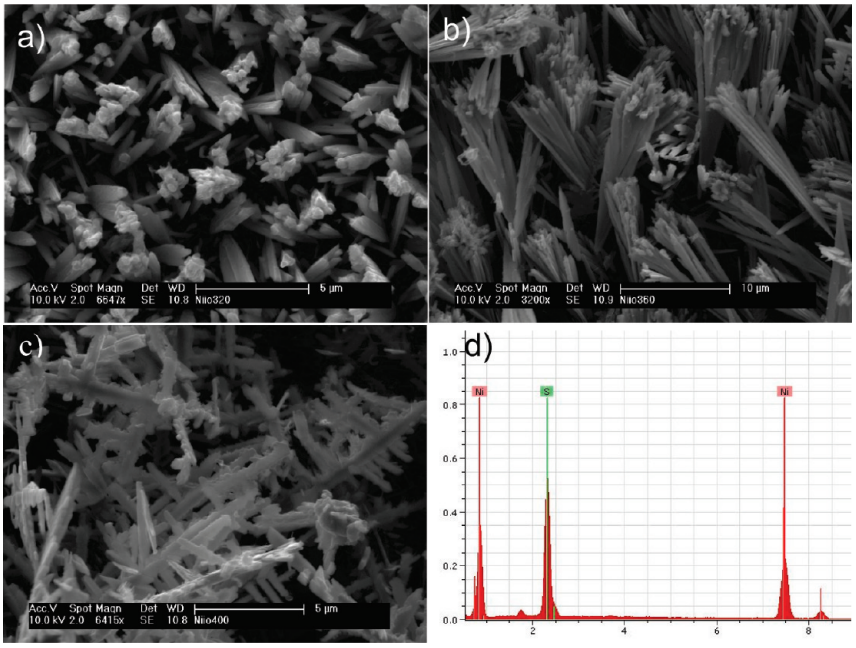

Figure 14. SEM images of films deposited from $[Ni(SON(CN^{i}Pr_2)_2)_2]$ (**4**) on glass at (a) 320 °C, (b) 360 °C, and (c) 400 °C (d) EDX graph.

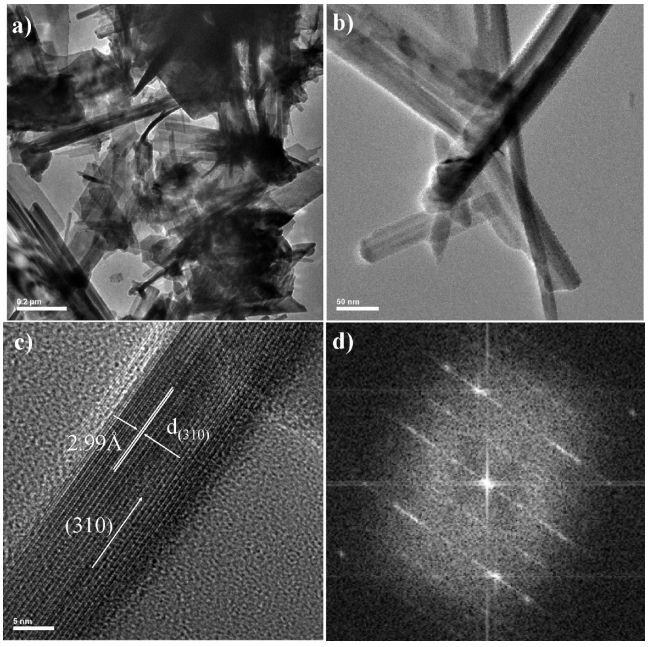

Figure 15. (a) and (b) TEM images, (c) HRTEM images (d) FFT pattern of nickel sulfide films deposited from $[Ni(SON(CN^{i}Pr_2)_2)_2]$ (**4**) on glass at 400 °C.

The SEM images of the films (Figure 17) show that the morphology of the nickel sulfide is dependent on the growth temperature. Films deposited at 360 °C consist of wormlike crystallites with an average length of 5 ± 1 μm and a width of 500 ± 25 nm. At 400 °C the films were composed of plates (4 ± 0.3 μm, length and 200 nm in width), whereas at 440 and 480 °C, smaller uniform rods were deposited with an average width of 200 ± 30 nm (440 °C) and 250 ± 25 nm (480 °C) and several micrometers of length. EDX analysis of the films shows the composition as Ni:S ratio: 49.1:50.9 (360 °C), 49.3:50.7 (400 °C), 53.2:46.8 (440 °C), and 54.9:45.1 (480 °C).

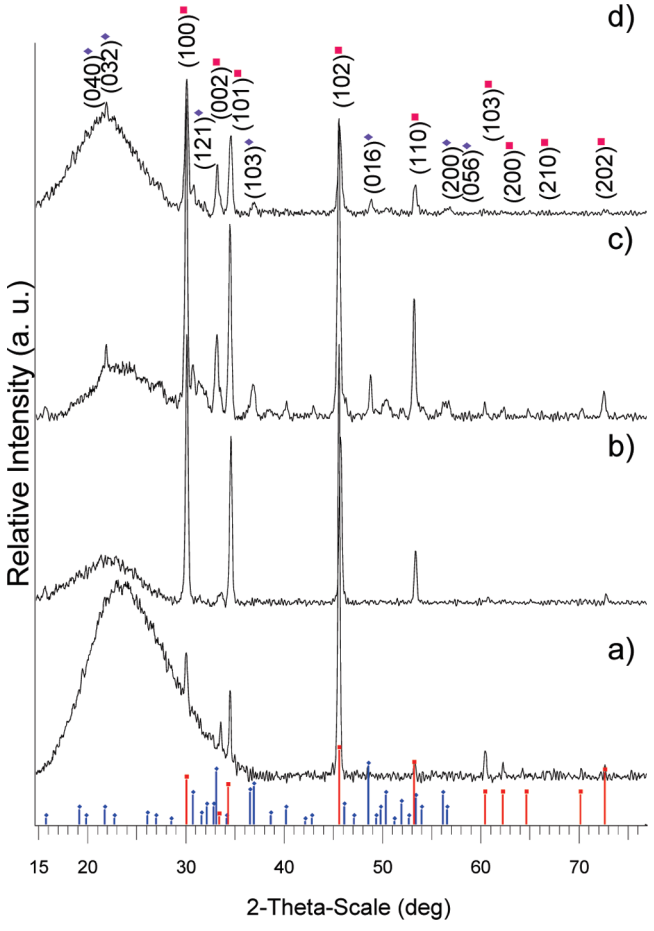

Figure 16. XRD pattern of nickel sulfide thin films deposited from $[Ni(N(SCNMe_2SCNEt_2))_2]$ (**6**) on glass at (a) 360 °C, (b) 400 °C, (c) 440 °C, and (d) 480 °C. Symbols (♦) indicating orthorhombic Ni_7S_6 (ICDD: 024-1021) and (■) indicating hexagonal $NiS_{1.03}$ (ICDD: 002-1273) phases.

The TEM images show the scratched crystallites from the film grown at 400 °C consist of nanobelts size ranging

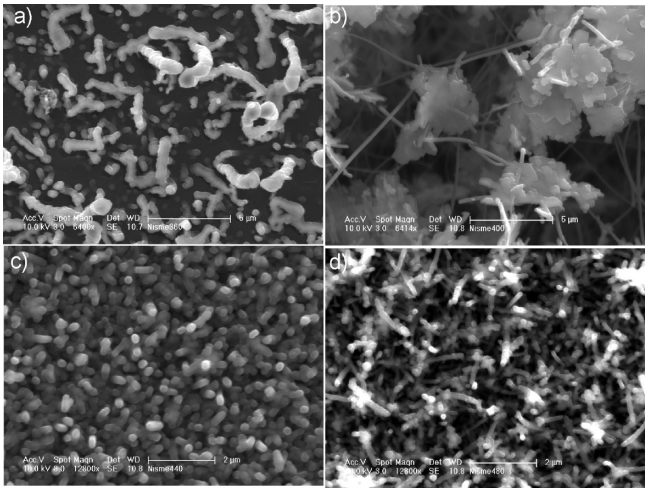

Figure 17. SEM images of films deposited from [Ni(N(SCNMe$_2$-SCNEt$_2$))$_2$] (**6**) on glass at (a) 360 °C, (b) 400 °C, (c) 440 °C, and (d) 480 °C.

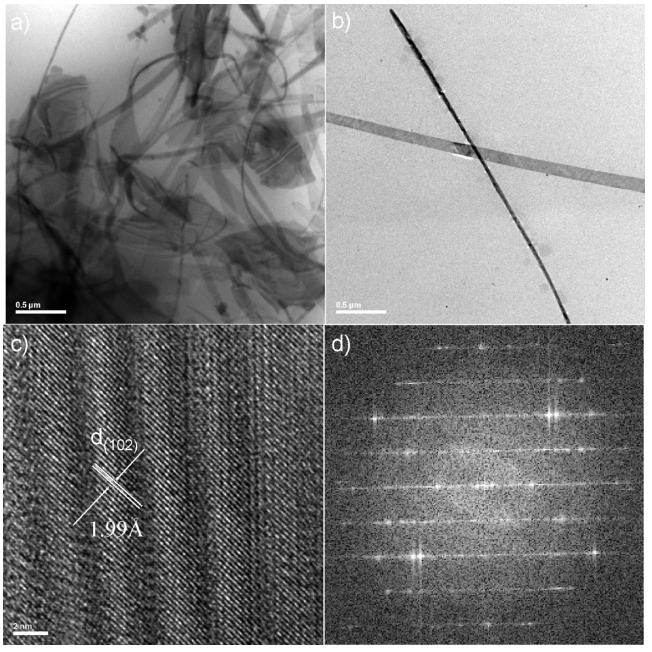

Figure 18. a) and b) TEM images, (c) HRTEM images and (d) FFT pattern of nickel sulfide films deposited from [Ni(N(SCNMe$_2$SCNEt$_2$))$_2$] (**6**) on glass at 440 °C.

from ca. 150 to 200 nm (Figure 18(b)). HRTEM images of the nanobelts (Figure 18(c)) show the lattice fringes with a *d*-spacing 1.99 Å corresponding to (102) reflection of hexagonal $NiS_{1.03}$, and the FFT pattern in Figure 18(d) shows the single crystalline nature of nanoplates.

Deposition of Nickel Sulfide Thin Films from [Ni(N-(SCNEt$_2$)$_2$)$_2$] (7). Thin films of nickel sulfide have been deposited from complex (**7**) in the temperature range of 360 to 480 °C on glass substrate. Black adherent uniform films were deposited at all temperatures. The X-ray diffraction (XRD) patterns of as deposited films at temperature between 360 and 480 °C are shown in Figure 19. At 360 and 400 °C NiAs hexagonal $NiS_{1.03}$ is obtained with major diffraction peaks of (100), (002), (101), (102), and (110) planes (ICDD: 002-1273). The XRD pattern from films deposited at 440 and 480 °C show diffractions

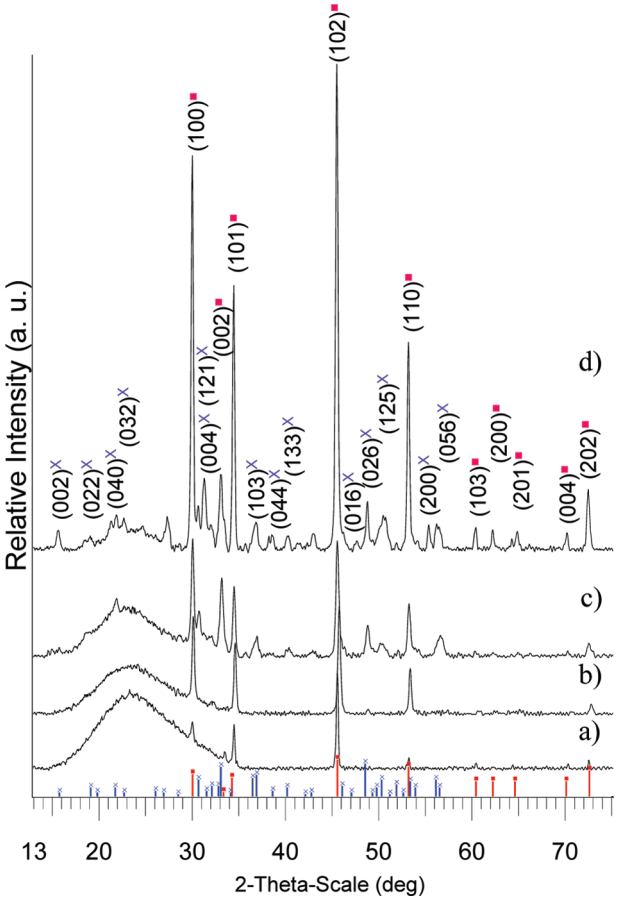

Figure 19. XRD pattern of nickel sulfide thin films deposited from [Ni(N(SCNEt$_2$)$_2$)$_2$] (**7**) on glass at (a) 360 °C, (b) 400 °C, (c) 440 °C, and (d) 480 °C. Symbols (x) indicating orthorhombic Ni_7S_6 (ICDD: 024-1021) and (■) indicating hexagonal $NiS_{1.03}$ (ICDD: 002-1273) phases.

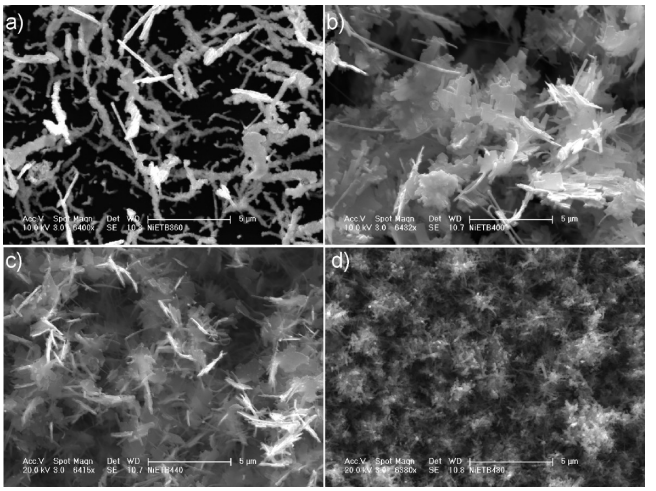

Figure 20. SEM images of films deposited from [Ni(N(SCNEt$_2$)$_2$)$_2$] (**7**) on glass at (a) 360 °C, (b) 400 °C, (c) 440 °C, and (d) 480 °C.

of hexagonal $NiS_{1.03}$ and also major peaks of (004), (121), (103), and (133) planes from orthorhombic Ni_7S_6 (ICDD: 024-1021) similar to films deposited from complex (**6**).

The SEM images of the films (Figure 20) show that the morphology of the nickel sulfide deposited at 360 °C consists of irregular rodlike crystallites with an average length of 6 ± 1 μm and a width of 600 ± 50 nm. At 400 and

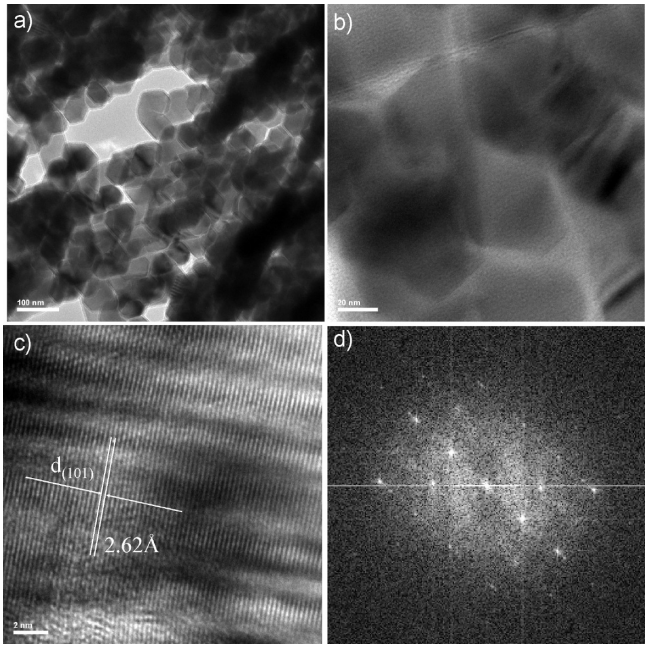

Figure 21. (a) and (b) TEM images, (c) HRTEM images (d) FFT pattern of nickel sulfide films deposited from $[Ni(N(SCNEt_2)_2)_2]$ (**7**) on glass at 440 °C.

Table 1. Summary of AACVD Results of Nickel Sulfide Thin Films Deposited Using Different Precursors

precursor	temperature °C	materials deposited	morphology
$[Ni(SON(CNMe_2)_2)_2]$	320	Ni_7S_6	wires
	360	Ni_7S_6	wires + plates
	400	Ni_7S_6	wires + plates
	440	Ni_7S_6	rods with pillar
$[Ni(SON(CNMe_2CNEt_2))_2]$	320	$Ni_{17}S_{18} + Ni_7S_6$	wires
	360	$Ni_{17}S_{18} + Ni_7S_6$	plates
	400	$Ni_{17}S_{18} + Ni_7S_6$	wires
	440	$Ni_{17}S_{18} + Ni_7S_6$	sheets
$[Ni(SON(CNEt_2)_2)_2]$	320	$Ni_{17}S_{18} + Ni_7S_6$	irregular
	360	$Ni_{17}S_{18} + Ni_7S_6$	plates
	400	$Ni_{17}S_{18} + Ni_7S_6$	plates
	440	$Ni_{17}S_{18} + Ni_7S_6$	plates
$[Ni(SON(CN^iPr_2)_2)_2]$	320	Ni_9S_8	flowers
	360	Ni_9S_8	flowers
	400	Ni_9S_8	branched
$[Ni(N(SCNMe_2SCNEt_2))_2]$	360	$NiS_{1.03}$	worms
	400	$NiS_{1.03}$	plates + wires
	440	$NiS_{1.03} + Ni_7S_6$	rods
	480	$NiS_{1.03} + Ni_7S_6$	rods
$[Ni(N(SCNEt_2)_2)_2]$	360	$NiS_{1.03}$	rods
	400	$NiS_{1.03}$	plates + wires
	440	$NiS_{1.03} + Ni_7S_6$	plates
	480	$NiS_{1.03} + Ni_7S_6$	rods

440 °C films of 4 ± 0.3 μm sized plates and 200 nm width sized wires deposited, whereas at 480 °C smaller uniform rodlike crystallites deposited with an average width size of 200 ± 20 nm. EDX analysis of the films shows the composition as Ni:S ratio: 49.2:50.8 (360 °C), 49.3:50.7 (400 °C), 55.5:44.5 (440 °C), and 56.1:43.8 (480 °C).

The TEM images show the scratched crystallites from the film grown at 480 °C consist of hexagonal nanoplates size ranging from ca. 35 to 40 nm (Figure 21(a)). This hexagonal primary structure attached side wise together to form a secondary rodlike crystallites. HRTEM images of the hexagonal plates (Figure 21(b) and (c)) show the lattice fringes with a *d*-spacing 2.66 Å corresponding to a (101) reflection of hexagonal $NiS_{1.03}$, and the FFT pattern in Figure 21(d) shows the single crystalline nature of hexagonal plates.

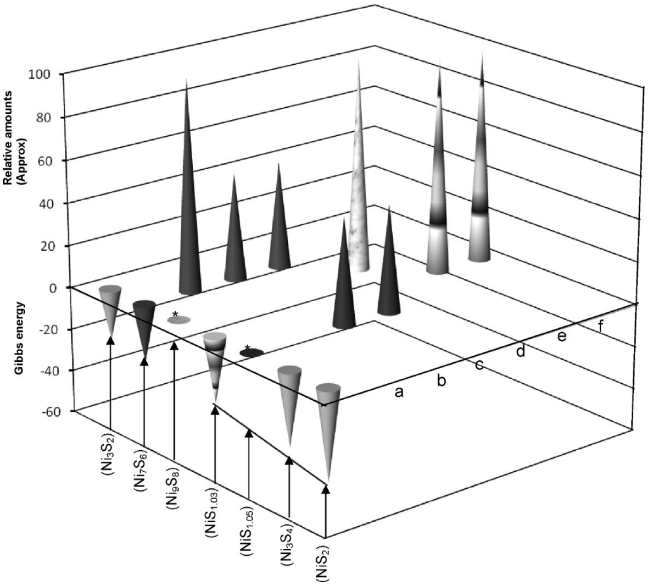

Figure 22. The phases nickel sulfide thin films deposited at 400 °C from a) $[Ni(SON(CNMe_2)_2)_2]$ (**1**), b) $[Ni(SON(CNMe_2CNEt_2))_2]$ (**2**), c) $[Ni(SON(CNEt_2)_2)_2]$ (**3**), d) $[Ni(SON(CN^iPr_2)_2)_2]$ (**4**), e) $[Ni(NS(CNMe_2CNEt_2))_2]$ (**6**), and f) $[Ni(N(SCNEt_2)_2)_2]$ (**7**), compared to the relative thermodynamic stabilities (ΔG) of the various phases of nickel sulfides calculated using heat of formation (ΔH) and entropy (ΔS) values taken from ref 32. Symbol (*) indicating unavailable thermodynamic data.

Conclusion

We have synthesized a series of new nickel(II) complexes of 1,1,5,5-tetraalkyl-2-thiobiurets (R = methyl (**1**); methyl, ethyl (**2**); ethyl (**3**); isopropyl (**4**)) and 1,1,5,5-tetraalkyl-2,4-dithiobiurets (R = methyl (**5**); methyl, ethyl (**6**); ethyl (**7**)). The single crystal structure of complexes (**1**), (**3**), (**4**), (**6**), and (**7**) were determined. In the case of the thiobiuret complexes the ligands coordinated *via* the S_2O_2 donor set with the two sulfur and two oxygen atoms are each mutually *cis*. Nickel is in square planar coordination in all seven thio and dithiobiuret complexes. AACVD from complex (**1**) deposited the orthorhombic Ni_7S_6 phase at all temperatures with spherical tipped wirelike crystallites at 320 °C, plates and wires at other temperatures. Complex (**2**) deposited a mixture of hexagonal $Ni_{17}S_{18}$ and orthorhombic Ni_7S_6 with wires and plates of crystallites. Similarly complex (**3**) also deposited a mixture of hexagonal $Ni_{17}S_{18}$ and orthorhombic Ni_7S_6 phases but with platelike crystallites, whereas complex (**4**) deposited an orthorhombic Ni_9S_8 phase with flowerlike crystallites at 320 and 360 °C, branched structures at 400 °C. Complex (**6**) gave NiAs hexagonal type $NiS_{1.03}$ at 360 and 400 °C, orthorhombic Ni_7S_6 phase at 440 and 480 °C with wires of spherical particles. Similarly complex (**7**)

(32) Mills, K. C. Thermodynamic data for inorganic sulphides, selennides and tellurides; Butterworth & Co., (Ltd.): London, England, 1974.

also deposited hexagonal $NiS_{1.03}$ at 360 and 400 °C, orthorhombic Ni_7S_6 phase at 440 and 480 °C, but with rods of crystallites composed of hexagonal plates. The composition of films deposited from all complexes was confirmed by EDX analysis.

The growth results for the deposition of nickel sulfide films from thiobiuret (**1**−**4**) and dithiobiuret (**6,7**) are summarized in Table 1. The relative stabilities of various phases of nickel sulfide are shown in Figure 22. The height of the cones on the negative *z*-axis represents the free energy of formation of each phase at 400 °C calculated using heat of formation and entropy values taken from ref 32. The phase deposited from the thiobiuret precursors (**1**−**4**) was Ni_7S_6, whereas the dithiobiuret precursors (**6,7**) deposited $NiS_{1.03}$. In this composition range NiS to NiS_2 are the most stable phases in a thermodynamic sense. The deposition of the 'subsulfide' Ni_7S_6 ([Ni]:[S] = 1:0.86) from thiobiuret probably reflects the lower sulfur content than in the dithiobiuret which leads to $NiS_{1.03}$. These observations are in stark contrast to the related tris-chelated iron complexes which deposit FeS or FeS_2, the two thermodynamically stable members of the series running from FeS to FeS_2.[33] None of the nickel precursors lead to the thermodynamically stable phase (NiS_2); however the kinetic phase Ni_7S_6 is observed in this system.

Acknowledgment. K.R. is grateful to ORS and The University of Manchester for financial support. The authors also thank EPSRC, UK for the grants to POB that have made this research possible.

Supporting Information Available: Crystallographic information files (CIF) for compounds **1, 3, 4, 6**, and **7** as electronic copies. This material is available free of charge via the Internet at http://pubs.acs.org.

(33) Ramasamy, K.; Malik, M. A.; Helliwell, M.; Tuna, F.; O'Brien, P.; *Inorg. Chem.* **2010**, *49*, 8495.